9-1-1999

Modeling of Solid Phase Detonations

C Richter

Hendrik J. Viljoen
University of Nebraska-Lincoln, hviljoen1@unl.edu

N.F.J Van Rensburg
Department Mathematics, University of Pretoria, Pretoria, South Africa.

International Journal of Self-Propagatilzg High-Temperature Synthesis
Volume 8, Number 3, 1999

Modeling of Solid Phase Detonations

C. Richter', H.J. Viljoen[1], and N.F.J. van Rensburg[2]

[1]*Department of Chemical Engineering, University of Nebraska-Lincoln, Lincoln, NE 68588-0126, U.S.A.*
[2]*Department of Mathematics and Applied Mathematics, University of Pretoria Pretoria, 0002 South Africa*

In contrast to conventional explosives which constitute rapid decomposition of the molecular structure accompanied by the release of large volumes of gaseous products, heterogeneous mixtures in the SHS realm react by progression of a thermal wave at velocities far below the speed of sound in such mixtures. Interestingly, ultrafast solid phase reactions can be initiated under the right conditions. A shock wave compresses the solid mixture to densities well beyond the theoretical mean ambient density (TMD) and compression becomes the major form of preheating. In addition, elastic potential energy is pumped into the lattice structure to induce severe distortion and eventually a structural collapse of the lattice on the atomic scale. Mixing and reaction proceed as in a dense gas and condensed products form. A continuum model is presented which addresses the following elements in the process. Compaction of the porous preform is described by an amended equation of state which includes plastic yielding and dilatation. The equation of state of densified material is based on an isobaric modification of the Mie-Gruneisen equation of state to account for anomalous behavior - a phenomenon of density reduction in the shock wave. Pressure is coupled into the kinetics as suggested by Benderskii insofar the activation energy is reduced proportionally to the stored elastic potential energy. Examples are presented of anomalous shock behavior, stable and unstable detonations.

Key words: *Coinpaction, impact, SHS, supersonic propagation.*

1. INTRODUCTION

Our understanding of solid phase reactions is far from complete. This is underscored by growing experimental evidence of chemical-mechanical interactions which cannot be explained within the conventional framework of diffusion and thermal conduction as the primary transport mechanisms which are responsible for reactant mixing and chemical activation in the solid phase. A few examples of chemical-mechanical interaction help to illustrate the broad impact of these interactions.

The synthesis of Grignard reactant in sonic reactors is significantly faster than in the absence of acoustic excitation **[1].** The direct modification of the magnesium surface by the pulsating pressure waves is credited for the enhanced rates. Reactive milling is another example [2]. A charge of Ti/C can be converted to TiC in a ball mill under prolonged milling where favorable conditions are created at the mesoscopic level upon impact of the milling media. The low probability of an impact with sufficient energy in the presence of both reactants make this conversion process very slow. However, the number of impacts which induce lattice distortions is much higher and the material becomes more reactive as the lattice defect concentration increases. A cornmonality is shared with sonic synthesis insofar as both processes induce lattice defects. In reactive milling considerable potential energy is pumped into the system by transforming it fromcrystalline to plastic and ultimately an amorphous state is approached (so-called metallic glasses). The metallic glass is much more reactive and conversion to TiC proceeds readily. Low temperature studies of certain polymerization reactions have also revealed an interesting chemical-mechanical interaction. Barelko et al. **[3]** investigated the chlorination of butylene at 77K and 4K, respectively. A conversion wave propagated through the solid mixture with little difference in velocity between the two temperatures. A fracture wave precedes the conversion, producing radicals, ions, and electrons in the crack surface which convert to product without thermal activation. Benderskii et al. **[4]** investigated the constancy of the reaction rate under these cryogenic conditions, pointing to a tunneling mechanism that supersedes thermal activation processes below certain temperature limits. They proposed a phonon modification of the reaction energy surface, where the phonon modes are excited by mechanical stresses. In a simplistic continuum description it can be described by a reduction of the activation energy of the rate limiting step as follows:

$$E = E_o - \epsilon_c = E_o + \int_{v_o}^{v} P_c dv \tag{1}$$

The activation energy is reduced by an amount equal to the elastic potential energy stored in the system. In practice this encompasses the modification from crystalline to plastic to glassy states as well as the compression of a crystal lattice. Another model has been proposed by Luty and Eckhardt [5]. The crystal lattice is susceptible to both mechanical and electronic coupling. In a shock wave, energy is stored in a phonon bath and is subsequently transferred into molecules, primarily as vibrational energy. Since certain phonon modes couple the energy more efficiently (so-called doorway modes), the creation of vibrationally hot molecules over macroscopic distances ensues. Excited states are reached where the decomposition of the structure follows naturally. As a first step to utilize this model in a continuum description, a linear relation as Eq. (1) offers a good starting point (Luty and Eckhardt, eg., (5.2)) [5].

A final example of mechanical-chemical interaction is shock-induced reactions. An excellent review of shock-induced chemical reactions was made by Thadhani [6]. The phenomenological processes which occur prior to shock-induced reaction is 1) formation of defects; 2) plastic deformation, void collapse and heating due to viscoplastic flow; **3)** turbulent-like flow with intense

mixing; 4) fissure and cracking to exposed surfaces with dangling bonds. Thadhani also notes that energy released in shock-induced reactions is primarily in the form of heat, however the melting temperatures of reactants or products are not always exceeded and condensed phase reactions are commonly found, for example, W and Re reaction [7]. The exact mechanism (or mechanisms) of the reaction is still not clear, and several kinetic models have been proposed by Thadhani [6] and Horie and-Kipp [8]. Temperature dependence is of the Arrhenius type and-the order of the reaction is usually first order if mixtures are assumed to be homogeneous. Horie and Kipp [8] considered a two-step mechanism with the formation of an intermediate product, followed by a transformation to the final product. The first step is a two-body interaction, which describes the mixing of reactants. The frequency factor for this step is varied linearly with the strain rate to account for the influence of hydrodynamical motion on mass mixing, but the basis for this is empirical. Bennett et al. [9] used this kinetic model in a heterogeneous system, finding reasonably good agreement with experimental systems Ni-Al and Al-Fe_2O_3. A more detailed description of the particle-particle interaction is given by Yano and Horie [10]. This description is based on discrete element modeling (DEM), an approach that accounts for the tracking of individual particles, similar to a molecular dynamics model. DEM reveals that particle velocity distributions could reach kinetic energy levels that could cause submicron-level mixing, thus providing the driving mechanism for ultrafast chemical reactions in the shock front. The validity of an Arrhenius-type model is questionable. Benderskii et al. [11] and experimental results by Enikolopyan [12] indicate that activation energy is lowered by elastic compression of reactants. This phenomenon is included in this paper. Mention should also be made of the important contributions of Enikolopyan and co-workers [12, 13]. His findings are based on experimental work done with a variety of materials in a Bridgman anvil. Wafers of solid material were placed in a die and loaded longitudinally or transversely. Reactions were initiated in the samples and extremely high conversion rates were observed. In one instance Al/Fe_2O_3 was compressed and ignited; the reaction was so violent that the die was destroyed. The system can also be dynamically loaded and the compression can cause sufficient preheating to ignite the system. Dynamic compression can be accomplished by imparting a shock to the system through a flyer plate or direct explosive charge. Shock dissipation can be countered by the release of chemical energy. The chemical energy couples back into the system in the form of thermal and kinetic energy to drive the shock. In a series of experiments by Gogulya et al. [14, 15], the Al/S system was compressed by an explosive. The Al/S system was ignited by the shock wave and a reaction front propagated at $\approx$ 4,400 m/s through the system. Experimental measurements are severely restricted by the extreme conditions and the opaque conditions complicate spectroscopic analysis.

There are many chemical systems with large heat of reaction, but the reaction rates are so slow that they are not considered energetic materials. If the reaction rates of mixtures which are used in typical SHS systems can be increased to values which are commensurate with the propagating speeds ofmechanical perturbations, solid phase detonations can be contemplated. A drastic increase in product formation is expected. The material also becomes a candidate for applications usually reserved for the classic energetic materials with pressures and temperatures which would go well beyond the reference scale for chemical reactions as we know it today.

In this paper we present an analysis of the solid phase reacting system. Some of the key features of the model are the compaction of porous materials and compression of the solids and the contributions of compaction and compression to the thermal component of the internal energy. It is shown that a reactive system can be readily ignited by an impact, even in the absence of pre-heating. Steady detonation, unstable detonation, and anomalous shock behavior are demonstrated by examples.

2. MATHEMATICAL MODEL

In practice it is not possible to prepare a reactive mixture without pores and realistic models should account for initial densities below TMD values. Pores must be ejected in a compaction step that precedes the reaction. If this step is rate-determining, it determines the thickness of the front. Two problems are-faced when compaction is included in the model, A realistic description of compaction of a mixture must be found and the equation of state must be adjusted for the porous state. Various attempts have been made to describe the shock compression of porous solids. As Sheffield et al. [16] remarked, it is common practice to assume that porosity is a function of pressure and empirically combine it into the porosity portion of the Hugoniot. In doing this, Hermann [17] accounted for elasticlplastic strength in a purely empirical way that requires calibration. Carroll and Holt [18], Carroll et al. [19], Merzhievskii and Tyagel'skii [20] and others attempted to include the elastoplastic effects in a less empirical way. Only the P-a model, in nearly the form originally presented by Hermann, has seen widespread use. However, it is still necessary to "guess" the function $\alpha(P)$. Simple linear forms are often sufficient, given the quality of experimental equations of state (EOS) (Sheffield et al. [16]). Fomin and Kiselev [21] proposed a sophisticated model to describe pore collapse, including elastoplasticity of the material. In reference to the mathematical models which are currently used, a model that allows for elastic and plastic behavior during the pore collapse phase and depends on the rate of deformation should suffice. This model is incorporated into a set of partial differential equations. A spatial grid of 10 pm and time steps of the order 10-100ps enable us to resolve the shock front and calculate physical quantities like pressure, velocity, conversion etc. in the shock front. This approach is in contrast to a popular alternative: pde's are solved on both sides of the shock front, connected by jump conditions which are consistent with the Rankine-Hugoniot equations. What the latter approach gains in expediency, is forfeited in the lack of resolution of the shock zone. The jump conditions should also account for transient effects and the unsteady Rankine-Hugoniot equations should be employed. A cautionary note about our approach is necessary. Discontinuities in initial and boundary conditions lead to discontinuities in the solution and the situation arises where solutions in the classical sense no longer exist. Consequently we have formulated the initial and boundary conditions to avoid such an occurrence.

Consider a mixture of reactive powders, pressed into the shape of a cylinder. In this analysis it is assumed that the powder has been compressed to a density p, which is less than the theoretical density of the system p, - a state with no pores present. The cylinder is placed in an ampoule and it is further assumed that the walls of the ampoule are rigid and perfectly insulating (adiabatic system). A one-dimensional description of the system, coinciding with the axial variable of the cylinder is used. The mixture is exothermic and the activation energy is in the order of 10^5 J/mole. In an Euler framework the cylinder has an initial velocity and at $t = 0^+$ it impacts with a wall. The ensuing shock wave consists of a leading part where elastic/plastic deformation of the porous phase occurs. Once the material is consolidated, it is assumed that the material immediately goes to a plastic state where stress is described by the three (equal) principal components and stress is substituted with the state variable pressure. Thus we assume that the initial potential energy due to elasticity of the solid phase has been converted into heat and the residual stress is zero.

Strictly speaking one should distinguish between all different (immiscible) phases of the system, because the material response would be different for each species. Particle velocities change rapidly in the shock front and in a multiphase model the particle velocity of each species is different. This gives rise to intense vortices and local mixing, a rapid exchange of momentum occurs, and within a

Table *1*

Property	Value	Units
E	10^5	J/mole
K_{i0}	80×10^9	Pa
L	10×10^{-6}	m
ρ_{i0}	2300	kg/m^3
C_v	925	J/kg·K
$(-\Delta H)$	3.1×10^6	J/mole
k	31.35	W/m·K
k_0	10^9	s^{-1}
T_0	298	K
σ_Y	80	MPa
α_T	5.0×10^{-5}	K^{-1}
χ	6.1	
μ	10.0	Pa·s

small distance the phases reach mechanical equilibrium. Likewise the temperatures ofdifferent species are not equal and thermal equilibrium is established in a time that depends on thermal conduction and particle sizes. This complexity is not included in the current model, hence perfect mixing is assumed and no distinction is made between different phases. The model is constructed around the reaction

$$4B + C \rightarrow B_4C.$$

Where possible the physical parameters have been selected for this system. However, we allow ourselves some latitude in the selection of some parameters, especially the isothermal bulk modulus, in order to explore the effect of these parameters on the solution. When no published data for some parameters could be found, values have been used which should be of similar magnitude (see Table 1 for parameter values).

The material is compressible, a necessary requirement when pressures of several hundreds of thousands atmospheres are present. The coupling of compression in the thermal component of internal energy plays a key role in initiating the chemical reaction. **A** distinction must be made between the bulk density p and the density of material ρ_i. The porosity is defined as

$$\alpha(x,t) = \frac{\text{Volume of particles + Volume of pores}}{\text{Volume of particles}}$$

It follows that the initial porosity is $\alpha_o = \frac{\rho_s}{\rho_o}$. The continuity equation is

$$\frac{\partial \rho}{\text{at}} + \frac{\partial(\rho u)}{\partial x} = 0, \tag{2}$$

where u denotes particle velocity of the material. The momentum balance can be written as

$$\frac{\partial(\rho u)}{\partial t} + \frac{\partial(\rho u^2)}{\partial x} = \frac{\partial \sigma}{\partial x}, \tag{3}$$

where a denotes the axial stress. The concentration balances are expressed in terms of mass fractions:

$$\frac{\partial(\rho X_B)}{\partial t} + \frac{\partial(\rho u X_B)}{\partial x} = -k_o 4 \frac{M_B}{M_C}(\rho X_B)(\rho X_C) e^{-\frac{E}{RT}}. \tag{4}$$

$$\frac{\partial(\rho X_C)}{\partial t} + \frac{\partial(\rho u X_C)}{\partial x} = -k_o(\rho X_B)(\rho X_C) e^{-\frac{E}{RT}}. \tag{5}$$

It is also necessary to model the axial stress a, taking into account the material response to stress. It is assumed that ρ_s remains constant during the porous phase and hence $p = \frac{P_s}{a}$. When the material is in the porous state, the axial stress is the sum of elastic and dissipative stress components, i.e. $\sigma = \sigma_{el} + \sigma_{disp}$. The elastic stress component is

$$\sigma_{el} = \frac{E_Y}{\alpha}\left[\frac{\alpha}{\alpha_o} - 1\right] \tag{6}$$

and the dissipative component has a form similar to dilatation in solids and liquids

$$\sigma_{disp} = \frac{4\mu}{3\alpha}\frac{\partial u}{\partial x}. \tag{7}$$

If the material is compressed to a certain threshold where a,, reaches the yield stress a,, it is assumed that

$$\sigma = \sigma_{disp} = \sigma_Y + \frac{4\mu}{3\alpha}\frac{\partial u}{\partial x} - \Phi(\alpha)P_T. \tag{8}$$

Every contribution to the total axial stress is now of a dissipative nature. The last term accounts for thermal pressure. Note that it depends on the porosity as given by the function $+(a)$. This will be discussed in greater detail at a later stage.

Once a reaches the value of one, the material no longer contains any pores at that point and the following equation of state (EOS) is used:

$$-\sigma = P = P_C + P_T - \frac{4}{3}\mu\frac{\partial u}{\partial x}. \tag{9}$$

This EOS consists of a cold-compression term (P,), a thermal term $(P,)$ and dilatation. An accurate description of the cold-compression or elastic part of the EOS offers most difficulty. There are marked differences in high pressure effects of gases and solids. The pressure in a gas is of thermal origin and is directly proportional to temperature. The compressibility of a gas is much bigger than for a solid

and the limiting compression $\frac{\gamma + 1}{\gamma - 1}$ (γ is the polytropic coeffient) is achieved across a shock wave of tens or a few hundreds of atmospheres. The behavior of a condensed phase to compression is altogether different. Under ambient conditions atoms maintain an average distance from each other to equilibrate attractive binding and repulsive nuclear forces. The cold compression of solids leads to huge internal pressures caused by repulsive nuclear–forces, In additions the material is strongly heated by a shock wave leading to additional pressure rise of a thermal origin. The thermal component of the pressure consists of nuclei vibration and electron thermal pressure. Shchetinin (1991) proposed a two-term equation of state for solids and liquids. The first term accounts for isothermal compression (P, component) and the second term P_T accounts for thermal contributions. Let K_{To} denote the bulk modulus of isothermal compression at the initial temperature and $\chi = 1 + \frac{\partial K_{T_o}}{\partial P}$ then P_c is given by

$$P_c = \frac{K_{T_o}}{\chi}\left[e^{\chi(1-\rho_s/\rho)} - 1 \right]. \tag{10}$$

This equation can be compared to alternative expressions like the Murnaghan equation:

$$P_c = \frac{K_{T_o}}{\chi - 1}\left[\left(\frac{\rho_s}{\rho}\right)^{1-\chi} - 1 \right].$$

The contribution from the electrons to the overall pressure only becomes significant above tens of thousands of degrees Kelvin. Neglecting this effect, thermal pressure is given by

$$P_T = \alpha_T K_{T_o}(T - T_o). \tag{11}$$

where α_T is the linear thermal expansion coefficient. The EOS (cf. Eq.(9)) can be written as

$$-\sigma = \frac{K_{T_o}}{\chi}\left[e^{\chi(1-\rho_s/\rho)} - 1\right] + \alpha_T K_{T_o}(T - T_o) - \frac{4}{3}\mu\frac{\partial u}{\partial x}. \tag{12}$$

It is assumed that α_T, K, and p are constant.

Returning to Eq. (8), the thermal pressure P_T is strictly speaking only relevant in the solid phase. However, to avoid a discontinuity (nonexistence of classical solution) and to compensate for the expansion of the matrix material during the compaction phase, we introduce the thermal pressure at an earlier stage using a "kick-in" function Φ. This function can be arbitrary as long as it is a smooth function that introduces thermal pressure over a small range of density $6 \leq p \leq 1$. We use a hermite cubic polynomial and choose $6 = 0.99$.

The internal energy balance is:

$$\frac{\partial(\rho\epsilon + \rho u^2/2)}{\text{at}} + \frac{\partial(\rho u[\epsilon + u^2/2])}{\partial x} = \frac{\partial(\sigma u)}{\partial x} + (-\Delta H)k_o(\rho X_B)(\rho X_C)e^{-\frac{E}{RT}} + \frac{\partial}{\partial x}k\frac{\partial T}{\partial x}. \tag{13}$$

A brief discussion of the internal energy E is necessary. In the consolidated state the internal energy consists of the elastic component ϵ_c and thermal component ϵ_T. The material does not accumulate elastic

potential energy during the compaction phase and only ϵ_T is present. The elastic and thermal components of internal energy can be expressed in terms of temperature and density:

$$\epsilon = \begin{cases} \epsilon_T = C_v(T-T_o) & \rho < \rho_s \\ \epsilon_c + \epsilon_T = \int_{\rho_o}^{\rho} \frac{1}{\rho^2} P_c d\rho + C_v(T-T_o) & \rho \geq \rho_s \end{cases} \tag{14}$$

Remark: It is convenient to evaluate the integral in Eq. (14) in terms of specific volume $v = \frac{1}{\rho}$. Afterwards the integrand can be written in terms of p again. The following scales are introduced to render the equations dimensionless. The cold sonic velocity, $c_o = \sqrt{\frac{K_{T_o}}{\rho_o}}$ is used as a scale for velocity, i.e. $\frac{u}{\ }$. Pressure is scaled as P Let L denote a length scale still to be defined, then time can be scaled as $\frac{L}{c_o}$. The density is scaled with the fully dense solid state under ambient conditions, p_o. The dimensionless temperature is defined as $\frac{T - T_o}{T_a - T_o}$ where T_a denotes the adiabatic temperature at atmospheric pressure. The length scale L was chosen as 10×10^{-6}m. Although this length scale is not a natural choice for the system, this length accounts for at least ten particle diameters (it is assumed that particles are typically 1–2pm in diameter), also the continuum model breaks down at the particle diameter length scale. L was also chosen as the step size in the spatial discretization. Hence $\Delta x = 1$ after scaling.

The same symbols can be used without confusion for the scaled variables. In dimensionless form, the governing equations can be written as

Continuitv:

$$\frac{\partial \rho}{\partial t} + \frac{\partial(\rho u)}{\partial x} = 0 \tag{15}$$

Momentum:

$$i\frac{\partial(\rho u)}{\partial t} + \frac{\partial(\rho u^2)}{\partial x} = \frac{\partial \sigma}{\partial x} \tag{16}$$

Boron mass fraction:

$$\frac{\partial}{\partial t}[\rho X_B] + \frac{\partial}{\partial x}[\rho u X_B] = -4\frac{M_B}{M_C} Da(\rho X_B)(\rho X_C) e^{\gamma\left(\frac{T-1}{T+\omega}\right)} \tag{17}$$

Carbon mass fraction:

$$\frac{\partial}{\partial t}[\rho X_C] + \frac{\partial}{\partial x}[\rho u X_C] = -Da(\rho X_B)(\rho X_C) e^{\gamma\left(\frac{T-1}{T+\omega}\right)} \tag{18}$$

Equation of state:

$$\sigma = \begin{cases} \rho\lambda\left(\dfrac{1}{\rho\alpha_o} - 1\right) + \beta_4\rho\dfrac{\partial u}{\partial x} & \sigma < \sigma_Y \text{ and } \rho < 1 \\ \sigma_Y + \beta_4\rho\dfrac{\partial u}{\partial x} - \Phi(\rho)\beta_5 T & \sigma > \sigma_Y \text{ and } \rho < 1 \\ -\dfrac{1}{\chi}\left[e^{\chi(1-1/\rho)} - 1\right] - \beta_5 T + \beta_4\dfrac{\partial u}{\partial x} & \rho \geq 1 \end{cases} \tag{19}$$

Internal energy:

$$\frac{\partial}{\partial t}[\beta_3\rho T + \rho\epsilon_c + \rho u^2/2] + \frac{\partial}{\partial x}\left[\beta_3\rho u T + \epsilon_c\rho u + \frac{\rho u^3}{2}\right] = \frac{\partial(\sigma u)}{\partial x} + \beta_1 Da(\rho X_B)(\rho X_C)e^{\gamma\left(\frac{T-1}{T+\omega}\right)} + \beta_2\frac{\partial^2 T}{\partial x^2}. \tag{20}$$

Initial conditions

The initial conditions which are used in this study describes a sample traveling at constant velocity U_o and at $t = 0$ it impacts a rigid barrier. The initial conditions of the other functions are $T = \rho - \frac{1}{\alpha_{oo}} = X, -0.769 = X, -0.231 = a = 0$. Thus no preheating of the sample and residual stresses during preparation are considered.

Boundary conditions

At the impact boundary $x = l$, the velocity is prescribed:

$$u(l,t) = \begin{cases} u_o\cos\dfrac{\pi t}{2\tau} & t \leq \tau \\ 0 & t \geq \tau \end{cases} \tag{21}$$

τ is not to be confused with the impact time, it is a measure of the rigidity of the barrier. The velocity of the material at the impact point is brought to zero in finite, albeit very short, time. In this study we have used $\tau = 1$, i.e., the same time it takes a longitudinal acoustic wave to traverse a distance of 10 μm. No thermal energy is exchanged with the wall, i.e. $\frac{dT}{dx} = 0$.

The end furthest from impact is a moving boundary. The system has never been integrated long enough for waves to reach the free end, therefore the choice of conditions at the free end does not affect the solution. Thermal conduction, which implies infinitely fast heat propagation, does not affect the solution either, because the numerical method introduces a characteristic that propagates with finite speed through the system. Furthermore these effects on the temperature solution are negligible. Tracking the solution for longer times would require solving a moving boundary value problem.

3. NUMERICAL SOLUTION

Numerical modeling of reactive compressible flows are notoriously difficult. Most studies deal with reactive gaseous systems and the ideal gas law remains a popular equation of state. In this case the equation of state is quite different and the parameters of the system correspond to the solid state. The solution is limited to a single spatial variable, coinciding with the axial variable of the cylinder. A finite difference method is used to solve this problem. The flux corrected transport (FCT) method of Boris and Book [23] has proved to be an effective method to resolve the steep gradients which are present in the shock zone. The method can be briefly described by applying it to the convection equation (which is the core of all the relevant balances (2)–(5) and (13)):

$$\frac{\partial A}{\partial t} + \frac{\partial uA}{\partial x} = 0$$

Let [Af] denote the discretized set at time t and let δt be the time step. FCT is essentially a two-step process. First $\bar{u}_{i+1/2} = 0.5(u_i^t + u_{i+1}^t)$ is calculated, as well as the parameters

$$\epsilon_{i+1/2} = \bar{u}_{i+1/2}\,\delta t$$

$$\nu_{i+1/2} = 0.5(0.5|\epsilon_{i+1/2}| + 0.25(1 + \epsilon_{i+1/2}^2)). \tag{22}$$

Remarks: E must satisfy $|\epsilon| < 1$ (which determines an upper bound on δt and v must satisfy: $0.25(1 + \epsilon_{i+1/2}^2) \geq \nu \geq 0.5|\epsilon_{i+1/2}|$ to guarantee positivity and stability. Equation (19) reflects a choice of v midway between the two bounds. The first step is diffusive and the intermediate values $[\bar{A}_i]$ are calculated as follows:

$$[\bar{A}_i] = aA_{i-1}^t + bA_i^t + cA_{i+1}^t$$

where $a = \nu_{i-1/2} + 0.5\epsilon_{i-1/2}$, b = $1 - 0.5\epsilon_{i+1/2} + 0.5\epsilon_{i-1/2} - \nu_{i+1/2} - \nu_{i-1/2}$ and c = $\nu_{i+1/2} - 0.5\epsilon_{i+1/2}$.

Next anti-diffusion fluxes are calculated to correct the strong diffusion introduced in the first step. The anti-diffusion coefficients are: $\bar{a}_{i+1/2} = \nu_{i+1/2} - 0.5\epsilon_{i+1/2}^2$ and the raw anti-diffusive fluxes (uncorrected values) are R,+,,,= $a_{i+1/2}(\bar{A}_{i+1} - \bar{A},)$. Let S denote the sign of $(\bar{A}_{i+1} - \bar{A},)$ and B = min[$S(\bar{A}_{i+2} - \bar{A},+,)$, $|R,+,,|$, $S(\bar{A}_i - \bar{A}_{i-1})$]. The corrected fluxes are $C_{i+1/2}$ = Smax [0, B] and in the second step the diffusive step is corrected:

$$A_i^{t+\delta t} = \bar{A}, - C_{i+1/2} + C_{i-1/2}.$$

There are some adjustable parameters in this method (see Boris and Book [23] for details), for example the inequality mentioned in **Remarks** allows some variation in the calculation of v. In the anti-diffusive step no existing maximum or minimum value is accentuated and this is evident from the way B is determined.

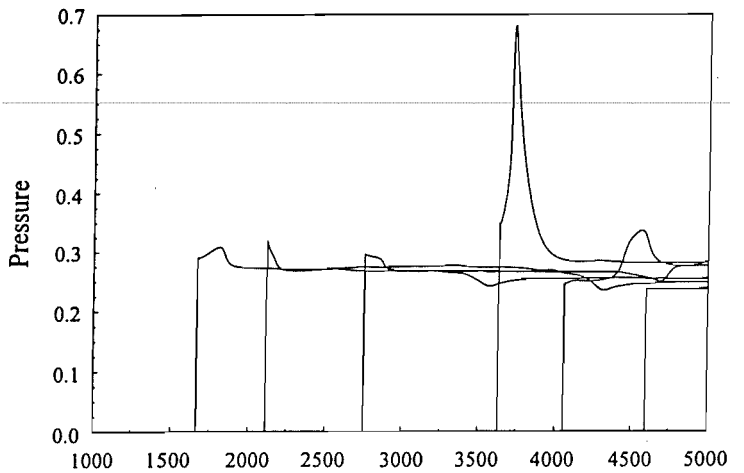

Fig. **1.** Pressure vs. time at (a) *100* pm and (b) *200* pm from the wall.

4. RESULTS

4.1. Unstable Detonation

Impact studies by Batsanov [24] on $Sn + S$ samples showed that partial conversion occurs in less than 10^{-7}s. Both elements have low isothermal bulkmodulii, compared to other typical SHS mixtures. To investigate the effect of low bulk modulus, a value of *20* GPa is selected. The dimensionless impact velocity is *0.3* and the system has an initial density of *0.8*. Figures *1-3* feature the pressure, density, and temperature profiles at six instances: $t = 600; 1400; 2000; 3000; 3800; 4400$. Note that the propagation is from right to left in these figures. At $t \leq 600$, the system appears to be in dynamic steady state and the shock wave is nearly constant. This is the only behavior that will be observed in samples which are short. The quasi-steady behavior is misleading though, because the system is still within an induction period before the ignition of the chemical reaction. The ignition occurs near the impact side and the reaction wave propagates at supersonic velocity towards the shock wave. Associated with the reaction front is a thermal pressure wave, noticeable as a hump in the pressure profile at $t = 1400$ in Fig. *1*. At $t = 2000$ the reaction wave has almost overrun the shock wave and strong interference results. Total pressure rises to $0.68K_{T0}$ ($\approx$ *136,000* atm.) and the combined front propagates with supersonic velocity. The detonation is not stable and the shock decays. At $t = 3000$ the pressure has receded to a value of ≈ 0.3 and only a small peak exists at the shock front. Over the duration of the last two profiles, the peak sharpens and broadens, a phenomenon that has also been observed for systems with no pores [25]). This effect is even more pronounced in the density profiles of Fig. *2*. The temperature profiles of $t = 2000$ and afterwards maintain a signature of the thermal peak which is associated with the brief detonation. This is understandable if one keeps in mind that the

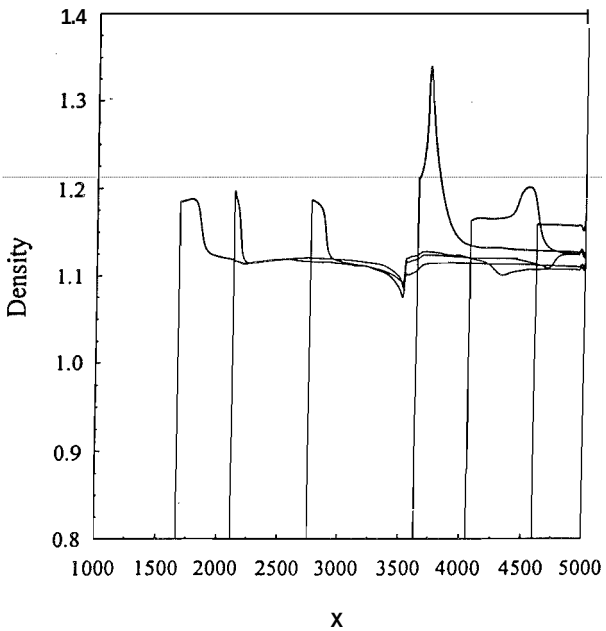

Fig. 2. Density vs. time at (a) 100μm and (b) 200 pm from the wall.

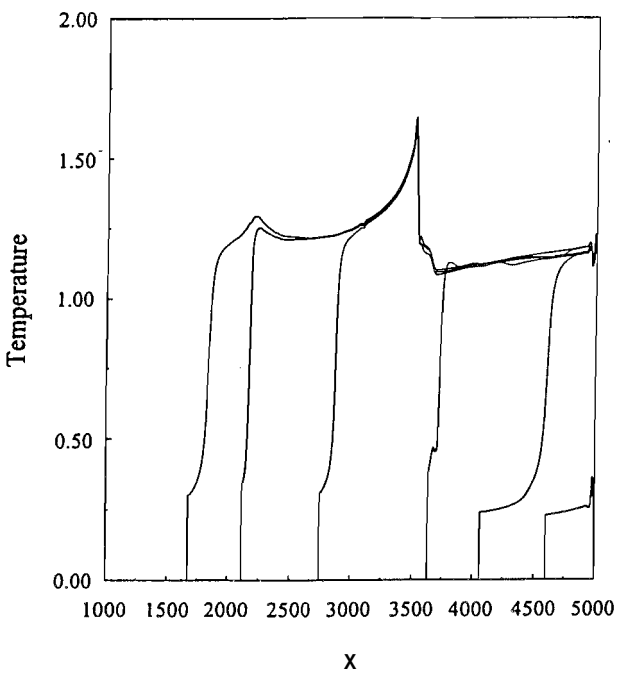

Fig. 3. Temperature (of solid Specimen) vs. time at (a) 100 μm and (b) 200 pm from impact point.

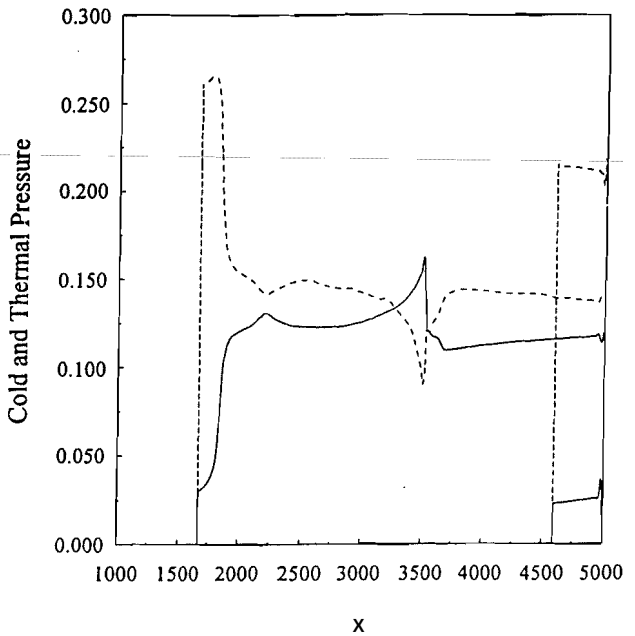

Fig. 4. Spatial profiles at time = 100, 200, 300, and 400 for (a) temperature and (b) boron mass function.

Eulerian framework is stationary with respect to the material behind the shock front (with theexception of some material flow due to density gradients). An interesting comparison is made in Fig. 4 between the two components of total pressure: P, and P_c (dashed line). The pressures are shown at $t = 600$ and $t = 4400$. During the induction period the cold pressure dominates thermal pressure. The profiles at $t = 4400$ shows a period where thermal pressure is larger than cold pressure and this coincides with the detonation period. **A** certain degree of symmetry exists between the profiles and this is reflected in the flatness of the total pressure behind the shock wave. The velocity of the shock wave is shown in Fig. 5. There is a slow increase that corresponds to the induction period, followed by a sharp rise to values of Mach 1.15 before the wave settles into a subsonic velocity of 0.75. When the numerical experiment is repeated for a bulk modulus of 80 GPa and the impact velocity is reduced to 0.15 (i.e., the absolute impact velocity remains constant) a qualitative similar solution is found — an induction period followed by a brief detonation and subsiding into a subsonic wave. Increasing the impact velocity to 0.3 and $K_s = 80$ GPa ($\alpha = 1.25$) did not lead to any detonation. **A** constant subsonic wave speed is approached shortly after impact and the reaction front tracks the shock wave with complete conversion. Temperature, pressure, and density profiles mimic traveling Heaviside functions. Except for a thin region in the shock front, the cold pressure is less than the thermal pressure with values 0.078 K_s and 0.21 K_s, respectively.

4.2. **Stable** Detonation

Two examples of stable detonation are presented. Their transient behavior differs during the period before steady state is reached. The first example has parameter values $K_s = 20$ GPa, $a = 1.1$

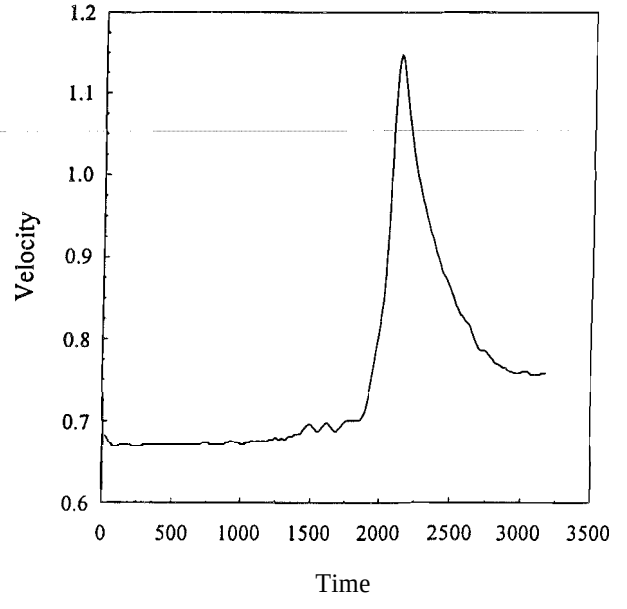

Fig. 5. Spatial profiles at time = 100, 200,300, and 400 for (a) pressure and (b) density.

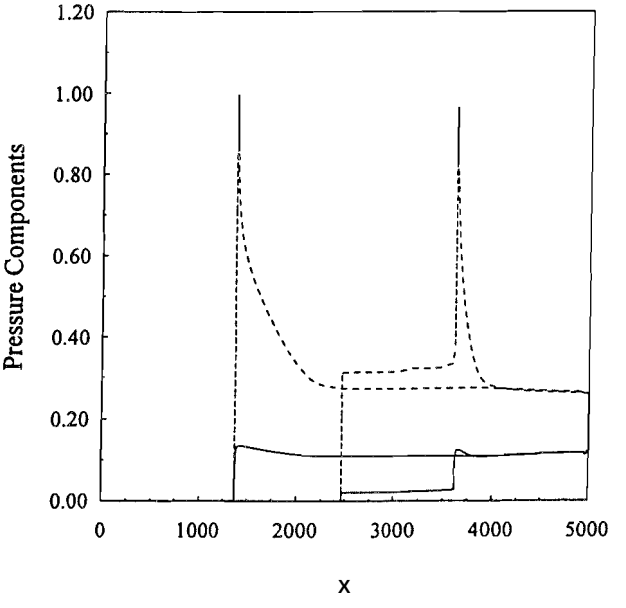

Fig. 6. Spatial profiles at time = 100, 200, 300, and 400 for (a) temperature and (b) boron mass function.

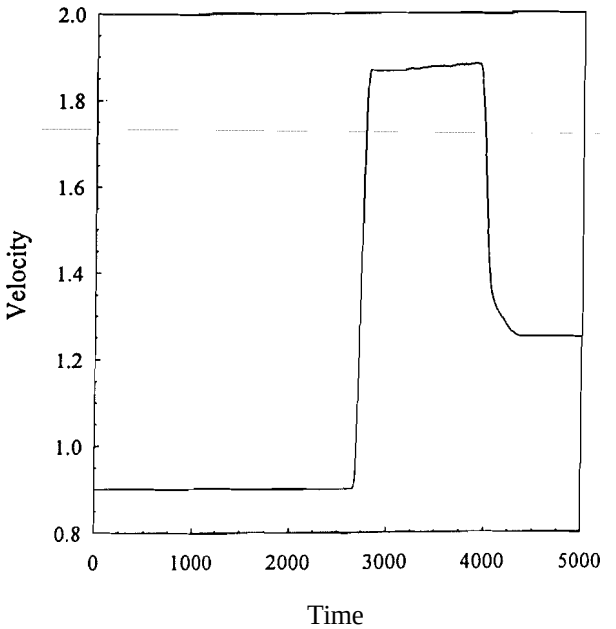

Fig. 7. Spatial profiles at time = 100, 200, 300, and 400 for (a) pressure and (b) density.

and the impact velocity is 0.3. In Fig. 6, the pressure components are shown at t = 2,800 and t = 4,000. The cold pressure is always larger than the thermal pressure. The thermal pressure at t = 600 shows the two major forms of heat generation. The initial thermal pressure rise is due to compression. This wave travels at Mach 0.9 through the porous medium. A stronger thermal pressure rise is associated with the position of the reaction front. The cold pressure also rises across the compression wave followed by a further increase across the reaction front. Both pressure components contribute positively towards the total pressure.

In Fig. 7 the velocity of the pressure peak is presented. The first period of $\approx$ 2,700 time units the maximum pressure is associated with the compression wave traveling at Mach 0.9. At the end of the induction period a pressure peak develops in conjunction with the reaction front. This front travels at supersonic speed and constitutes a detonation. The detonation wave overruns the compression wave and speeds it up to a steady velocity of Mach $\approx$ 1.25. The system exhibits delayed ignition and overshoot. When the numerical experiment is repeated for K_{To} = 20 GPa, a = 1.1 and a higher impact velocity of 0.5, the transient behavior is much shorter. The pressure, temperature, and density all resemble traveling Heaviside functions and the compression wave is tracked by the reaction front. An interesting result though, is that the propagation velocity is lower, Mach $\approx$ 1.1, which is 442 m/s slower than impacting the system at lower speed of 0.3. The difference is the exact position of the reaction front. In the former case it overran the compression wave and in the process accelerated it. **At** higher impact velocity the heat generated by the compression wave is sufficient to ignite the reactants. However, the reaction front is not pushing the compression front — this is a consequence of the compression wave, but does not provide feedback.

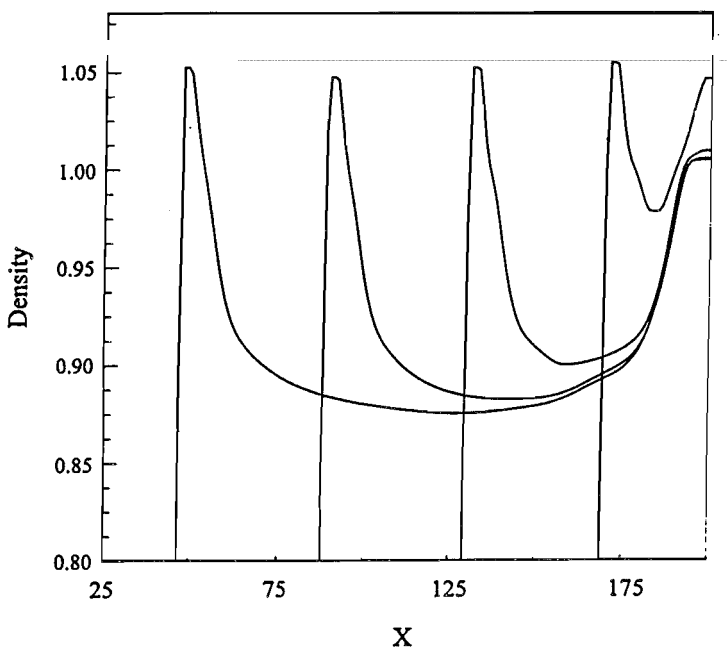

Fig. 8. Temperature profiles at time = 100, 200, 300, and 400 (no chemical reaction).

4.3. Anomalous Behavior

This curious effect was first observed experimentally by Kormer et al. [26] and Krupnikov et al. [27] with shock compression of porous metals. The thermal component of internal energy is responsible for expansion of material. Increased porosity leads to an increase in thermal internal energy and above certain porosities the thermal pressure dominates cold pressure and the density is less than TMD. The following set of conditions is used: $K_{To} = 25$ GPa, $a = 2.25$ and impact velocity is 0.4. In Fig. 8 the density profiles are shown at four instances, t = 100; 200; 300; 400. The material is compressed in the shock front to values slightly above TMD, this implies that all pores have been ejected from the medium. The reaction heat and heat from compression lead to thermal expansion and the density drops to values as low as 0.875 TMD. The pressure components are shown in Fig. 9. The thermal pressure completely dominates the cold pressure, the latter is only significant in the leading edge of the compression wave where it is responsible for the ejection of pores. The propagation velocity is subsonic.

The distended state behind the shock front does not contain any pores and the EOS of the solid state must be used. The classic isochoric arguments on which the Mie-Gruneisen equation rests become contentious for the distended state, because it is argued that cold pressure now becomes negative and the descriptions for $P_c(\rho)$ generally fail at negative pressure. **An** isobaric approach as described by Wu

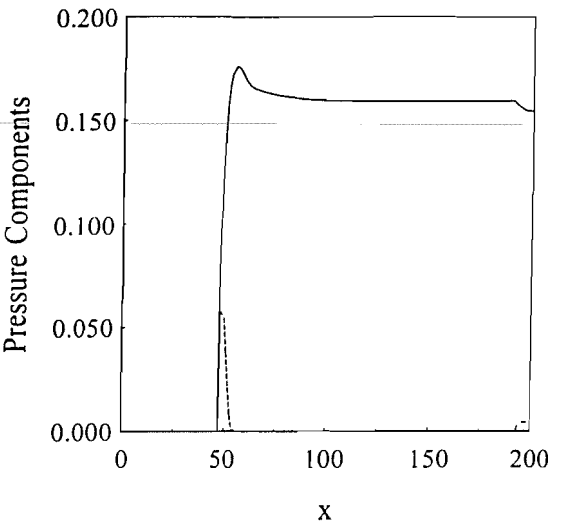

Fig. **9.** Anomalous behavior with thermal pressure (solid line) completely dominating cold pressure (dashed line).

and Jing [28] and Boshoff-Mostert and Viljoen [29] overcome this problem. The Mie-Gruneisen equation relates pressure contributions at a common specific volume:

$$P_T = P - P_C = \frac{\Gamma}{v_o} C_v (T - T_o). \tag{23}$$

An alternative viewpoint is to consider specific volume at a specific pressure as the sum of thermal and **athermal** components. The thermal component v_T is a function of pressure and temperature:

$$v_T = v - v_C = \frac{R}{P} C_P (T - T_o). \tag{24}$$

Both equations map out a surface in v $\times$ T $\times$ P space and these surfaces overlap except at moderate pressures and high temperatures (anomalous region). When the shock wave is treated as a discontinuity traveling at constant velocity, the conservation equations (mass, momentum and energy) can be integrated across the discontinuity and the resulting v-T-P values behind the shock front define a point on these surfaces. Varying the shock velocity, a locus is traced on the surfaces. When this curve is projected onto the P-v plane, it is referred to as a Hugoniot. The Hugoniots of the two approaches are given by the following two equations respectively:

$$P = \frac{\frac{v}{\Gamma} P_c - \epsilon_c}{\frac{v}{\Gamma} - \frac{1}{2}(v_{oo} - v,} \tag{25}$$

$$v = \frac{v_c - \frac{R}{P}(\epsilon_c + pv_c) + \frac{R}{2}v_{oo}}{1 - \frac{R}{2}}. \tag{26}$$

Both curves emanate from the point (P_o, $v_o = 1/(\rho_o s)$), pararneterized by the initial specific volume v_o. When $\frac{dP}{dv}|(P_o, v_s)| > 0$, the shock behavior is anomalous and the isobaric approach is superior to the Mie-Gruneisen approach. Of course $R(P)$ must still be determined. Equation (25) gives very accurate descriptions of Hugoniot data if the function $\Gamma(v)$ is known. The Gruneisen parameter relates the changes in phonon frequencies with changes in specific volume and this function of volume is approximated by the Slater equation [30] Eq. (11.18)).

Since R is not a function of a, one can equate the Hugoniots of Eqs. (25) and (26) for $a = 1$ to solve for $R(P)$. Afterwards $R(P)$ can be used in an EOS that follows from Eq. (24) and this EOS is valid for arbitrary initial porosities. A comparison between Eq. (26) and experimental anomalous behavior data of Trunin [31] is very good [29].

$$v - \frac{v_o}{\chi}\left[\chi - \ln\left(1 + \frac{P\chi}{K_{T_o}}\right)\right] - \frac{R}{P}C_P T = 0. \tag{27}$$

This EOS is a little more tedious to solve than Eq. (19c), because pressure is an implicit function of temperature and specific volume, but it can be resolved with almost no added computational effort.

ACKNOWLEDGMENT

HJV and CR acknowledge the financial support of the National Science Foundation through grant CTS-9900451.

Nomenclature

	Cold sonic velocity $\sqrt{KT_o/\rho_o}$
	Specific heat capacity at constant volume J/kg·K
Da	$\frac{k_o \mathrm{Le}^{-\gamma}}{c_o}$
E	Activation energy, J/mole
E_Y	Young's modulus, Pa
$(-\Delta H)$	Heat of reaction, J/mole
k	Thermal conductivity W/m.K
k_o	Pre-exponent rate constant, $m^3/kg \cdot s$
K_{To}	Bulk modulus of isothermal compression, Pa
L	Length scale, 10×10^{-6} m
$M_{B,C}$	Molar mass of boron/carbon, kg/mole
P	Pressure, Pa
R_g	Universal gas constant, J/mol·K
T	Temperature, K

t	Time, sec.
U	Particle velocity, m/s
V	Specific volume, m^3/kg
x	Axial coordinate, m
Y_o	Yield strength at room temperature, Pa

Greek Symbols

α_T	Coefficient of linear thermal expansion, K-'
β_o	$\frac{\mu}{\rho_o c_o L}$
β_1	$\frac{(-\Delta H) X_{fo}}{c_o^2}$
β_2	$\frac{k(T_a - T_o)}{L\rho_o c_o^3}$
β_3	$\frac{C_v(T_a - T_o)}{c_o^2}$
β_4	$\frac{4\mu_{To}}{3\rho_o L c_o}$
β_5	$\alpha_T(T_a - T_o)$
β_6	$\frac{Y_o}{\rho_o c_o^2}$
γ	$\frac{E}{R_g T_b}$
Γ	Gruneisen coefficient
ϵ	Internal energy, J/kg
h	Dimensionless Young's modulus, E_Y/K_{To}
χ	$1 + \frac{\partial K_{To}}{\partial P}$
μ	Viscosity coefficient, Pa·s
P	Density, kg/m^3
ω	$\frac{T_o}{T_a - T_o}$
σ	Axial stress

Subscripts

a	Adiabatic
c	Isothermal
o	Initial
s	Solid state
T	Thermal

REFERENCES

[1] C. Horst, et al., "Design, Modeling and Performance of a Novel Sonochemical Reactor for Heterogeneous Reactions," *Chem. Eng. Sci.*, vol. 51, p. 1837, 1996.

[2] V.V. Boldyrev, "Mechanical Activation and It's Application in Technology," *Mat. Sci. Forum*, vols. 269–272, p.227, 1998.

[3] V.V. Barelko, et al., "High Speed Autowave Reaction Regimes in Low-Temperature Solid State Chemistry," *Russ. Chem. Rev.*, vol. 59, p. 205, 1990.

[4] V.A. Benderskii, et al., "Limits of Fast and Slow Penetration of a Fluctuating Barrier in the Theory of Solid-Phase Cryochemical Reactions," *Dokl. Akad. Nauk SSSR*, vol. 311, p. 260, 1990.

[5] T. Luty, and C.J. Eckhardt, "General Theoretical Concepts for Solid State reactions: Quantitative Formulation of the Reaction Cavity, Steric Compression and Reaction-Induced Stress Using an Elastic Multipole Representation of Chemical Pressure," *J. Am. Chem. Soc.* vol. 117, pp. 2441-2452, 1995.

[6] N.N. Thadhani, "Shock-Induced Chemical Reactions and Synthesis of Materials," *Prog. in Mat. Sci.*, vol. 37, p. 117, 1993.

[7] N.N. Thadhani, A.H. Advani, E. Dunbar, H.A. Grebe and I. Song, "Shock-Induced Chemical Reactions in Wand *Re* Powder Mixtures," in *High Strain Rate Behavior of Refractory Materials*, eds. R. Ashafani, E. Chen and A. Crowson, TMS, Warrandale, PA (1991).

[8] Y. Horie and M.E. Kipp, "Modeling of Shock-Induced Chemical Reactions in Powder Mixtures," J. *Appl. Phys.*, vol. 63, no. 12, p. 5718, 1988.

[9] L.S. Bennett, Y. Horie and M.M. Hwang, "Constitutive Model of Shock-Induced Chemical Reactions in Inorganic Powder Mixtures," J. *Appl. Phys.* vol. 76, no. 6, p. 3394, 1994.

[10] K. Yano and Y. Horie, "A Numerical Study of Shock-Induced particle Velocity Dispersion in Solid Mixtures," J. *Appl. Phys.*, vol. 84, no. 3, p. 1292, 1998.

[1 I] V.A. Benderskii, P.G. Filippov, and M.A. Qvchinnikov, "Ratio of Thermal and Deformation Ignition in Low Temperature Solid Phase Reactions," *Doklady Akademii Nauk SSSR*, vol. 308, no. 2, pp. 401–405, 1989.

[12] N.S. Enikolopyan, A.I. Aleksandrov, E.E. Gasparyan, V.I. Shelobkov and A.A. Mkhitaryan, "Direct Conversion of Chemical Energy into Mechanical without Thermalization," *Doklady Akad. Nauk SSSR.* vol. 319, no. 6, p. 1384, 1991.

[13] N.S. Enikolopyan, "Super-fast Chemical Reactions in Solids," *Russian* J. *Phys. Chem.* vol. 63, no. 9, pp. 1261-1265, 1989.

[14] M.F. Gogulya, et al., "Interaction of Sulphur and Aluminum Behind Shock Fronts," *Khim. Fiz.* vol. *10,* pp. 420–425, 1991.

[15] M.F. Gogulya, et al., "Interaction of Sulphur and Aluminum Behind Shock Fronts," *Khim. Fiz.* vol. 11, pp. 224–229, 1992.

[16] S.A. Sheffield, et al., "Shock Loading of Porous High Explosives," in *Higlz-Pressure Shock Compression of Solids,* eds. L. Davison, Y. Horie and M. Shahinpoor, Springer, New York (1997).

[17] W. Hermann, "Constitutive Equation for the Dynamic Compaction of Ductile Porous Materials," *J. Appl. Phys.*, vol. 40, no. 6, pp. 2490–2499, 1969.

[18] M.M. Carroll, and A.C. Holt., "Static and Dynamic Pore-Collapse Relations for Ductile Porous Materials," *J. Appl. Phys.* vol. 43, no. 4, pp. 1626–1635, 1972.

[19] M.M. Carroll, K.T. Kim and V.F. Nesterenko, "The Effect of Temperature on Viscoplastic Pore Collapse," J. *Appl. Phys.* vol. 59, no. 6, pp. 1962–1967, 1986.

[20] L.A. Merzhievskii, and A.V. Tyagel'skii, "Modeling of Dynamic Compression of Porous Iron," *Comb. Explosives and Shock Waves,* vol. 30, pp. 522–530, 1994.

[21] V.M. Fomin and S.P. Kiselev, "Elastic-Plastic Waves in Porous Materials," in *High-Pressure Shock Compression of Solids,* eds. L. Davison, Y. Horie and M. Shahinpoor, Springer, New York (1997).

[22] V.G. Shchetinin, "Calculations of the State Parameters of Condensed Substances at High Pressures and Temperatures," *Comb. Expl. and Shock Waves* vol. 27, pp. 39–42, 1991.

[23] J.P. Boris, and D.L. Book, "Solution of Continuity Equations by the Method of Flux-Corrected Transport," *Methods in Computational Physics,* vol. 16, p.85, 1976.

[24] S.S. Batsanov, *Effects of Explosions on Materials: Modification and Synthesis under High-Pressure Shock Cotnpression,* Springer-Verlag, New York (1994).

[25] J.R. Bielenberg, and H.J. Viljoen, "Chemo-Mechanical Interaction in Solid-Solid Reactions," *AlChE Journal,* vol. 45, no. 5, pp. 1072–1084, 1999.

[26] S.B. Kormer, A.I. Funtikov, V.D. Urlin, and A.N. Kolcsnikova, "Dynamic Compression of Porous Metals and the Equation of State with Variable Specific Heat at High Temperatures," *Sov. Phys.-JETP*, vol. 15, no. 13, pp. 477–488, 1962.

[27] K.K. Krupnikov, M.I. Brazhnik, and V.P. Krupnikova, "Shock Compression of Porous Tungsten," *Sov. Phys. JETP*, vol. 15, no. 13, pp. 470–476, 1962.

[28] Q. Wu, and F. Jing, "Thermodynamic Equationof State and Application to Hugoniot Predictions for Porous Materials," *J. Appl. Phys.*, vol. 80, no. 8, pp. 4343–4349, 1996.

[29] L. Boshoff-Mostert, and H.J. Viljoen, "Comparative Study of Calculation Methods for Analytical Hugoniot Curves of Porous Metals," *J. Appl. Phys.* (to appear), 1999.

[30] Ya.B. Zel'dovich, and Yu.P. Raizer, "Physics of Shock Waves and High-Temperature Hydrodynamic Phenomena," vol. II, Academic Press, NY (1967).

[31] R.F. Trunin, "Shock Compression of Condensed Materials," Cambridge University Press, Cambridge, (1998).